N71-23518

NASA CR-118007

QUARTERLY REPORT

OCT.- DEC. 1970
JAN.- MARCH 1971

JET PROPULSION LABORATORY
CONTRACT #952 - 543

STUDY OF THE ZINC-SILVER OXIDE BATTERY SYSTEM

PRINCIPAL INVESTIGATOR
DR. LEONARD NANIS
ASSOCIATE PROFESSOR
SCHOOL OF CHEMICAL ENGINEERING
UNIVERSITY OF PENNSYLVANIA

This work was performed for the Jet Propulsion Laboratory, California Institute of Technology, sponsored by the National Aeronautics and Space Administration under Contract NAS7-100.

TABLE OF CONTENTS

SUMMARY

1.1. Electrode Studies

1.1.1. Porous electrodes

An optical method to detect the onset of the reaction zone at the rear of the porous electrode has been developed to speed up the evaluation of the electrochemical Thiele parameter. The Thiele parameter compares interface reaction resistance to electrolyte ohmic resistance. The optical luminance technique "senses" the nature of the granular material in the porous electrode because internal reflections and refractions cause wave length dependent absorption to occur in the diffusely scattered light. This scattering effect has been proven to extend into a depth of several thousandths of an inch from the rear of a porous material. When used with electrodes of various initial thickness, this optical method will permit the obtaining of information equivalent to several slicing and chemical analysis experiments. The advantage of working with a full size electrode under conditions which apply in battery operation is the ultimate goal of this work. This method is particularly well suited to studying transient effects such as pulse-charging.

1.1.2. Zinc Dendrites

A review of previous work has been continued. The net finding of researchers is that mossy deposits are obtained for activation controlled deposition, while dendritic deposits are

obtained when diffusion is the controlling step. Preliminary experiments have been continued with lead nitrate solutions and shadow Schlieren techniques to visualize concentration gradients at the tips of growing dendrites. Photographic studies by this method clearly show that lead dendrite formation involves natural convection. By comparing the Grashof number for the lead nitrate system with that for practical battery electrolytes, it has been estimated that the driving force for natural convection is negligible compared with the special case of the lead nitrate solution.

2.1. Membrane Permeation

The permeability of ZnO in 40% KOH through an acrylic acid grafted and divinyl benzene crosslinked polyethylene battery separator membrane has been determined by an improved technique. At 0.4 M ZnO concentration and 26.5°C, the permeability is 3.63×10^{-5} cm/sec. An unsteady-state technique is being developed that will allow rapid determinations of permeability for varying temperature and concentration in a single run.

2.2 Diffusivity of ZnO in 40% KOH

The new diffusivity apparatus has been completed and is being calibrated. An analysis of the flow characteristics of the equipment shows that with the new design the $\Delta\ell$ effect will be negligible and the end boundary condition will be satisfactorily met.

1.1. Electrode Studies

1.1.1. Porous electrodes

1.1.1.1. Introduction

The cycle life and performance of silver-zinc batteries is limited by the capabilities of the zinc electrodes. These negative electrodes limit cycle life because of changes in physical characteristics (particularly porosity) and/or because of the formation, during charge, of metallic dendrites which can penetrate the cell separators (1,2). In the design of a battery for a specific application, it is desirable to be able to specify the thickness and thus the weight of the electrodes so that excess material is not unnecessarily used. In order to be specific about a particular cycle life and depth of discharge, it is necessary to know the depth of penetration of reaction into the porous battery electrode i.e. the current distribution. There are many mathematical treatments for simplified systems, originally inspired by fuel cell reactions. For battery electrodes, the changing morphology adds complexity to the mathematics. These problems have scarcely been begun. For example, the formation of an insulating product completely changes the nature of current distribution within the pore structure. Also, gas evolution may contribute to a total re-arrangement of the current and also affect the resistance of the pathways within the porous electrode.

The data obtained on model configurations cannot be extrapolated to practical systems with any degree of confidence.

Consequently, detailed experiments on actual battery electrodes are necessary in order to determine current distribution under actual operating conditions. The ultimate goal of such studies is to assemble operating characteristics in the form of the Thiele parameter for various cycle behavior and temperatures, etc. so that batteries may be designed for specific applications.

1.1.1.2 Performance and cycle life

By considering the porous electrode to be the analog of chemical catalyst structures, Bro and Kang (3) have been able to characterize electrode behavior in terms of an electrochemical Thiele parameter. The electrochemical analog turned out to be the throwing power parameter in electrodeposition technology (2) modified by being multiplied by a ratio of particle diameter to electrode thickness.

The use of the electrochemical Thiele parameter to predict the penetration of reaction front into the porous electrode is a step ahead in rational electrode design (2).

The slicing method used by Bro and Kang (3) is tedious and produces results which average out important local variations caused by current distribution on a gross scale, such as across the width of the electrode.

The obvious advantages of the electrochemical Thiele parameter for practical engineering of battery systems are combined with a high speed method for profile determination.

The method,which has been explored in a preliminary way, is based on the determination of spectral luminance or diffuse reflection from the rear side of the porous electrode. By detecting the arrival of e.g. discharge at the rear of porous electrodes of various thicknesses by optical changes, the same discharge profile data as obtained from the slicing technique may be finally assembled.

The optical method will be able to map out the local distribution of reaction by limiting the light spot size and also will be able to follow the charge-discharge behavior of an electrode over many cycles under actual battery operation conditions.

1.1.1.3. Preliminary experiments

The possible hues and color variations of practical battery plates have been simulated with mixtures of two powders, namely black activated carbon and white alumina powder. The mixtures were wetted in acetone to simulate electrolyte.

The apparatus consists of two light paths within tubes with a light source at one end and a detector at the end of the other tube, both of which make an angle with the bottom of a shallow glass dish. Different powder mixtures were placed in the dish. A high intensity microscope lamp was used as an incandescent light source with intensity control provided by control of the voltage to the lamp.

The intensity of the diffusely reflected light from the material at the bottom of the dish was sensed by a silicon photo cell using a Keithley electrometer to measure the current. The angle of the incident light with the plane of the simulated electrode was arranged to avoid total reflection. A standard surface is used for comparison of reflections for luminance. White filter paper is suitable for this purpose. In the dry condition, various mixtures are readily distinguished by changes in the relative intensity of diffusely reflected light. When wet, the distinction is somewhat less but still permits clear resolution of a relative weight or volume fraction of each component of the mixture. By adding several layers of the calibrating paper, it was determined that six or seven thicknesses are needed to produce no further change in the diffuse scattering. This indicates that the light actually senses a depth of several thousandths of an inch of material so that it is certain that not just the final rear surface of the electrode is evaluated by this technique, but rather a region close to the final surface. Crude experiments were performed using colored filters with the silicon photo cell and incandescent light source to determine whether or not spectral sensitivities could be determined. Results are indeterminate at present since the filters are not classified according to spectral behavior. Further work along this line is being carried out.

1.1.2. Zinc dendrites

1.1.2.1. Introduction

In a previous report (2) there has already been discussed the literature work on zinc dendrite formation and the possible influence of natural convection on the morphology of zinc dendrites.

The presence of traces of impurity or slight changes in temperature, concentration, current density and applied potential may completely change both size and growth habit of crystal species. In addition, the surface of the actual electrode may vary in reactivity from point to point. It is important that these physical changes and their effect be detected and analyzed in terms of overall deposit structure.

1.1.2.2. Mass transfer and morphology

It has already been demonstrated (4) that diffusion plays an important part in the morphology of metal deposition. The rate of zincate diffusion and the occurrence of spherical or linear diffusion in relation to the geometry of the electrode-electrolyte interface controls both the overall growth rate and the selective propagation of individual dendrites (5). In a study of forced convection on the morphology of zinc, Stachurski (4) has used the rotating electrode. The rotating electrode offers certain advantages over stationary electrodes in that deposition is easier to control by adjusting limiting current with changes in rotational speed. The concentration of zincate at the surface of the rotating electrode remains constant during the experiment because of the uniform accessibility of the rotating disk electrode.

The diffusion coefficient and the concentration of zincate determine the diffusion limiting current in a well-defined hydrodynamic system.

Three different types of deposits can be distinguished

(a) smooth, obtained only on rotating discs at high Re, at overpotentials less than 100 millivolts and high concentration of zincate.

(b) foam, also called moss; a soft and weak deposit of whiskers. It is formed at low overpotentials (less than 100 millivolts) and at high concentration of zincate.

(c) dendrites, obtained in free electrolyte and usually at higher overpotentials than for (b).

The effects of natural convection on dendritic growth were studied in preliminary work (5) which involved controlled potential. It is somewhat more realistic to use constant current methods since batteries are normally charged in this manner.

Arouete and Blurton (6) have established two classes of zinc deposition in a free convection system: an activation controlled deposit, which has a mossy appearance, and a diffusion controlled deposit, which conformed to the more usual concept of a dendritic deposit. When zinc is deposited from zincate saturated KOH, a change in densities of the electrolyte occurs in the immediate vicinity of the electrode. The natural or free convection is due to the density differences which, for vertical electrodes, cause an upward or downward flow of the solution, depending on whether the density of the electrode layer is smaller or greater than the bulk.

1.1.2.3. Preliminary experiments

In a lead nitrate solution, one can observe Schlieren during deposition and dissolution (2). The Schlieren phenomenon has been further examined in an unstirred solution, using two optical methods.

For usual observation, a diffuse light source was employed. The test cell used in earlier experiments has been placed in a feasible optical arrangement with the diffuse light source. Photographs were taken(with a Nikon - 35 mm camera with close-up lenses)of the electrode during deposition and dissolution.

A shadow Schlieren method derived from thermal boundary layer studies has been adapted to get greater contrast photographs of concentration gradients associated with lead growth and dissolution (7). As with all Schlieren methods, light rays passing through a medium with a continuously variable index of refraction become deviated into optically denser parts of the medium. The image is formed by the projection of a shadow without the use of lenses. The optical arrangement viewed from above is shown in Fig. 1. It consists of a condenser lamp, plexiglass square sided cell (3" X 2" X 3"), matte glass screen adjacent to the cell, and Nikon-35mm camera, with close-up lenses. Photographs are taken of the image projected on to the matte screen.

Schlieren experiments have been combined with quantitative current-potential determinations during lead deposition. The apparatus and experimental technique used were similar to those used by Wilke et al(8) with the anode and cathode arranged vertically.Times on the order of 1 minute were allowed following each voltage step to insure steady current readings. Cathodic overpotential was measured with respect to a lead reference electrode dipping into the same solution, using a Luggin capillary probe. Lead deposits were examined at 30 magnifications, using a binocular microscope.

1.1.2.4 Results and discussion

The shadow Schlieren method was found to give the best contrast for lead deposition and dissolution Schlieren. Results are shown in figure 2a in appendix 1.1.2.1 for Schlieren which occurred during dissolution. The streaming is seen to follow a nearly vertical path downwards while the Schlieren in figure 2b during dendrite formation rise in an upward direction towards the free solution surface, where free convection circulation is established.[9] At higher net current density, the Schlieren become much more distinct than for lower currents. The results shown in figure 2 indicate clearly that both lead deposition and dissolution involve natural convection. At low current densities in the so called activation controlled region, the lead deposition has been found to consist primarily of whisker growth and it is this region where the Schlieren are very vague. At higher current densities where distinct dendrite formation occurs, the Schlieren are very pronounced. The extreme localization of the Schlieren at the tips of growing dendrites (Figure 2b, appendix 1.1.3.1) indicate an extremely non-uniform distribution of current density. The general linear shape of the current overpotential curve (Sec. 1.1.3.1: Figure 3) obtained during deposition from 0.73 M Pb $(NO_3)_2$ solution, indicates only an activation controlled region in current density range in which the photographs (Figure 2) are obtained. Thus, Schlieren associated with diffusion limitation and concentration overpotentials are visible in the activation controlled region.

Using the low current approximation to the overall electrochemical rate law (linear region), the exchange current density J_o, may be calculated from the slope in figure 3 using the relation $\partial\eta/\partial J = \frac{2F}{RT}\ \frac{1}{J_o}$ Eqn. 1

The exchange current density for lead deposition in 0.73 M $Pb(NO_3)_2$ is thus approximately 47 mA/cm^2. This value compares favorably with the exchange current density found by Piontelli(16) for single crystal (111) Pb electrodes in perchlorate electrolyte (0.5 M Pb $(ClO_4)_2$ + 0.5 M $HClO_4$), where J_o = 21 mA/cm^2 and also for sulfamate (0.5 M Pb $(NH_2SO_3)_2$ + 0.5 M NH_2SO_3H), where J_o = 52 mA/cm^2. Much further theoretical consideration must be directed to the problems of a) equivalent exchange current densities for electrolytes which result in totally different growth modes and b) the simultaneous occurrence of activation type of overpotential with mass transport limitations. Regarding the second question, quantitative measurements relating index of refraction profile and fraction of limiting current are needed.

The Grashof number is a non-dimensional group which combines the factors which describe the magnitude of natural convection. In a sense, the Grashof number compares as a ratio the magnitude of inertial to viscous forces which occur during natural convection. By evaluating this characterizing parameter for the lead nitrate system, it is possible to compare equivalent convective effects for other systems whose Grashof number is known. As it happens, the lead nitrate solution has the distinct advantage of a large change in refractive index as a function of concentration, thus making it possible to clearly observe natural convection. Other electrolytic systems of interest do not necessarily have such a large refractive index change. By comparison of Grashof number the possible existence of important convective effects may thus be estimated.

The dimensionless Grashof number, Gr, is defined by the relation(8,10)

$$Gr = \frac{g\ h^3 \Delta\rho}{\nu^2\ \rho} \qquad \text{Eqn. 2}$$

where: g = gravitational acceleration, cm/s^2; h = electrode height, cm; $\Delta\rho$ = density difference between bulk solution and interface, g/cm^3; ρ = average electrolyte density, g/cm^3 and ν = kinematic viscosity, cm^2/s. The density change is customarily included as the percentage variation of density with respect to concentration change in the densification coefficient α as given in Eqn. 3

$$\alpha = \frac{\Delta\rho}{\rho\Delta c} \qquad \text{Eqn. 3}$$

In electrolyte systems, the densification coefficient does not vary greatly with concentration, and thus serves as an overall convenient parameter for comparison of various solutions.

For a standard electrode height of 1 cm, the Grashof number for the lead nitrate system (0.73M) is approximately 9500 at 25°C, using standard density data (11), and estimating viscosity at 1.6 centipoise based on the viscosity of $CuSO_4$. Details of the calculation may be found in table 1, appendix 1.1.3.2. The Grashof number has been also calculated for a [$CuSO_4$ - H_2SO_4-H_2O] system. The details of the calculation are listed in table 2, appendix 1.1.3.2. Density and viscosity data for 0.7 M $CuSO_4$ solution in 1.5 M H_2SO_4 at 25°C were taken from the work of Eisenberg et al (12). For the standard electrode height of 1 cm, a Grashof number of approximately 7200 is found for the above mentioned system.

Of more direct interest to battery technology, the electrolyte composition for the silver-zinc battery is essentially saturated ZnO in 30% KOH solution. Using density and viscosity data taken from the work of Eisenberg (13), the Grashof number for deposition i.e. charging at 25°C for the electrode height of 1 cm is computed to be Gr = 1235. It is clear that the Grashof number for the practical silver-zinc battery system is much less than the equivalent Grashof number for lead nitrate or copper sulfate solution. As a consequence, natural convection should be expected to occur to a much lesser degree in the silver-zinc electrolyte.

In actuality batteries with separators between electrodes where the spacings are much less than 0.5 mm have geometric factors which strongly influence the natural convection.

Some idea of the effect of natural convection in narrow spacing may be found in the work of Böhm et al (15). For the narrow space enclosed between a vertical electrode and a diaphragm, the following generalized mass transport correlation (dimensionless) was obtained:

$$Nu = 0.0225 \left(\frac{a}{h}\right)^2 (Sc \cdot Gr)^{0.85} \qquad \text{Eqn. 4}$$

where Nu = Nusselt number $\left(\frac{kh}{D}\right)$; k = mass transfer coefficient, cm/sec; Sc = Schmidt number $\left(\frac{\nu}{D}\right)$; and a = electrode-diaphragm, cm. Equation 4 is valid in the range of $a < a_k$, where a_k corresponds approximately with the thickness of the mass transport diffusion layer. Where the separation between electrode and diaphragm is greater than a_k the more commonly encountered equation which relates Nusselt number with the Schmidt and Grashof number serves (8)

$$Nu = 0.67 \ (Sc \ Gr)^{1/4} \qquad \text{Eqn. 5}$$

Assuming typical values for electrode height of 4 cm and spacing of 0.2 mm between plate and diaphragm, the Nusselt number for the ZnO-KOH system for Sc=3900 (based on estimated $D = 5 \times 10^{-6}$ cm^2/sec), has a calculated value of 85 using equation 5. By including the geometric factor according to equation 4 the corresponding Nusselt number is 8.3. Thus mass transfer by natural convection in practical battery systems where constricted spacings occur is considerably lower than for the usual free electrolyte type of convection.

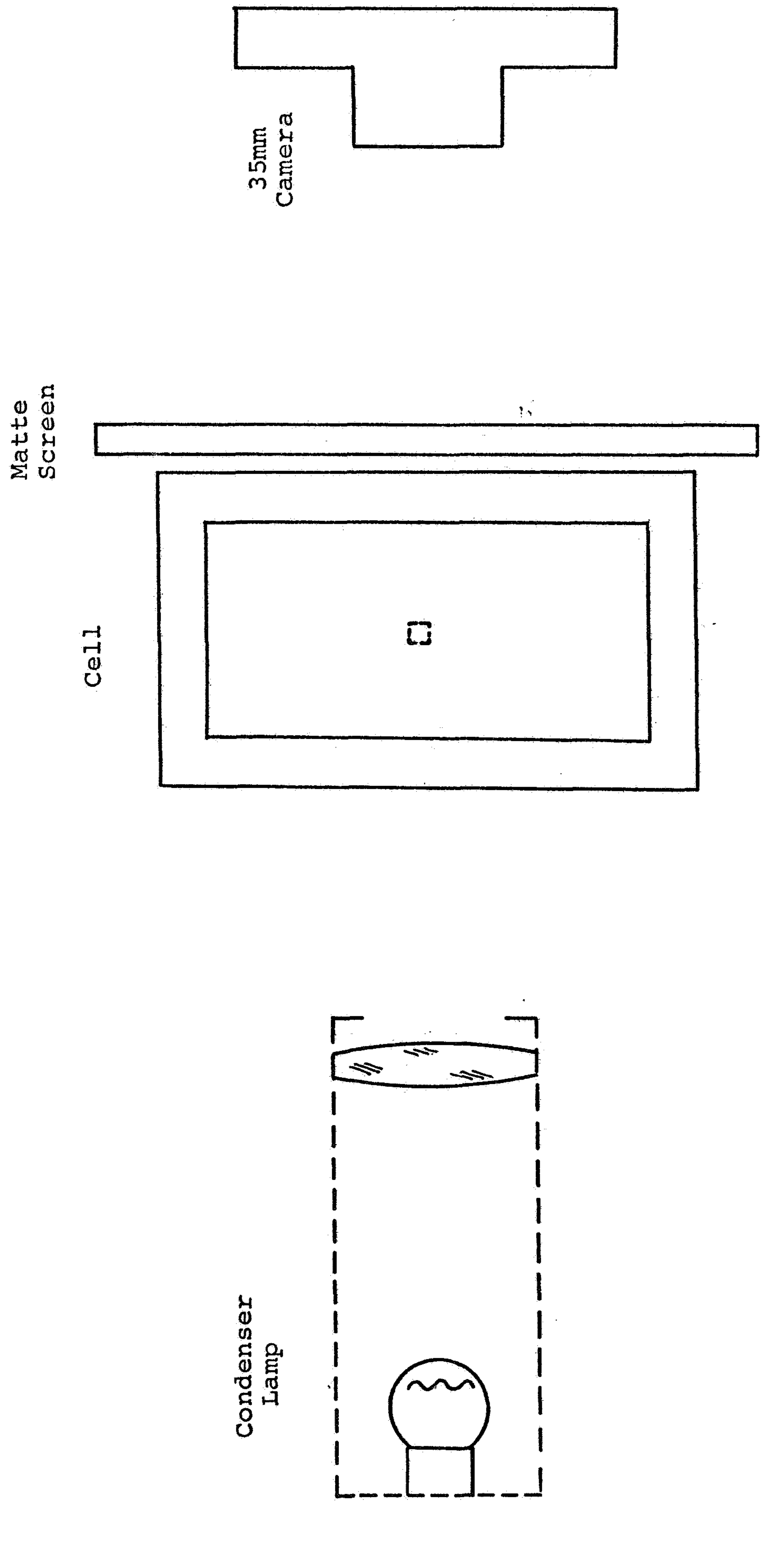

Figure 1 Optical arrangement of the shadow Schlieren method

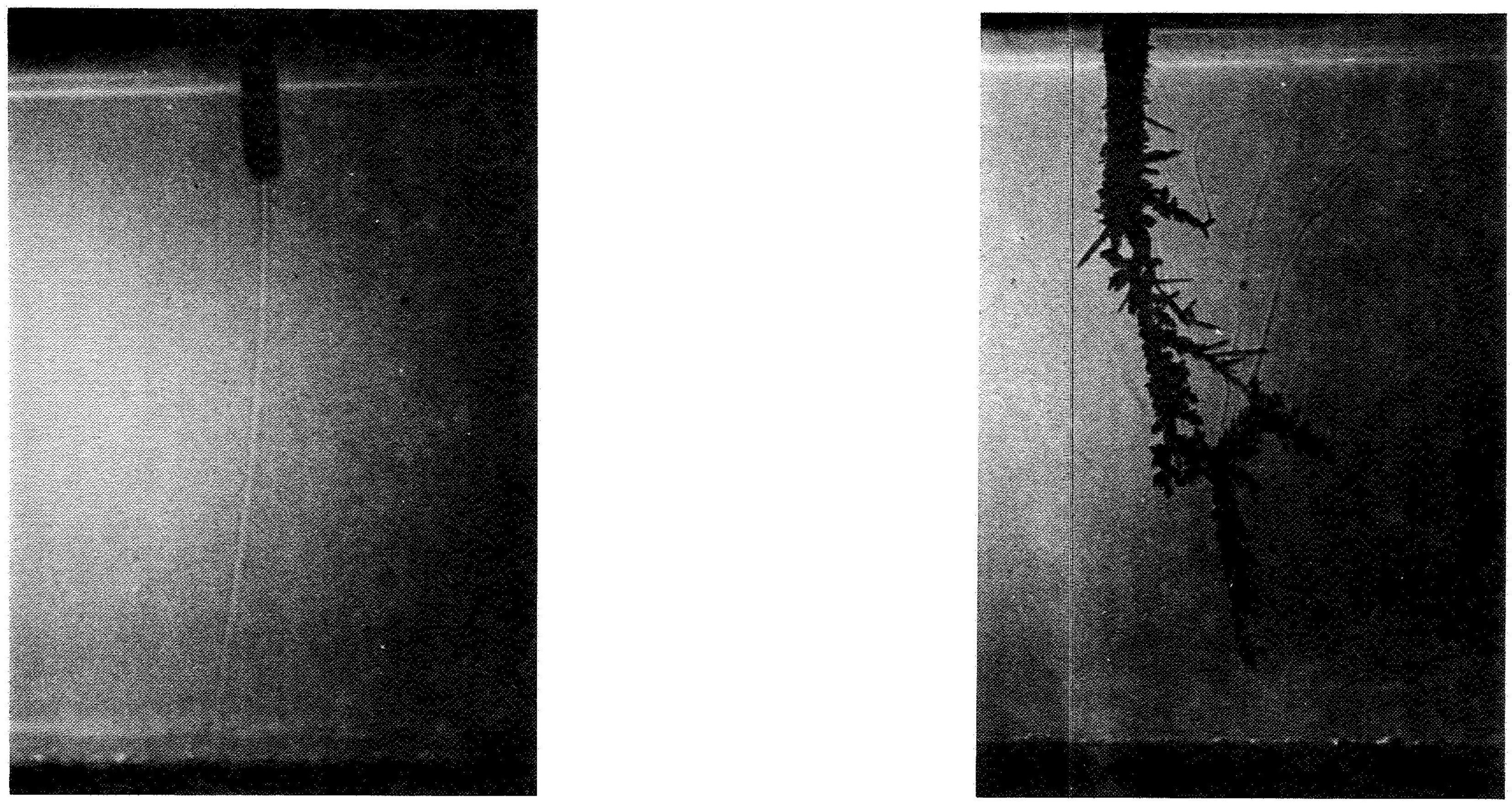

(a) (b)

Figure 2: Schlieren with the shadow Schlieren method

(a) dissolution in 0.73 M $Pb(NO_3)_2$ at c.d. 25 mA/cm^2

(b) deposition (dendritic growth) in 0.73 M $Pb(NO_3)_2$ at initial c.d. 50 mA/cm^2

FIG. 3

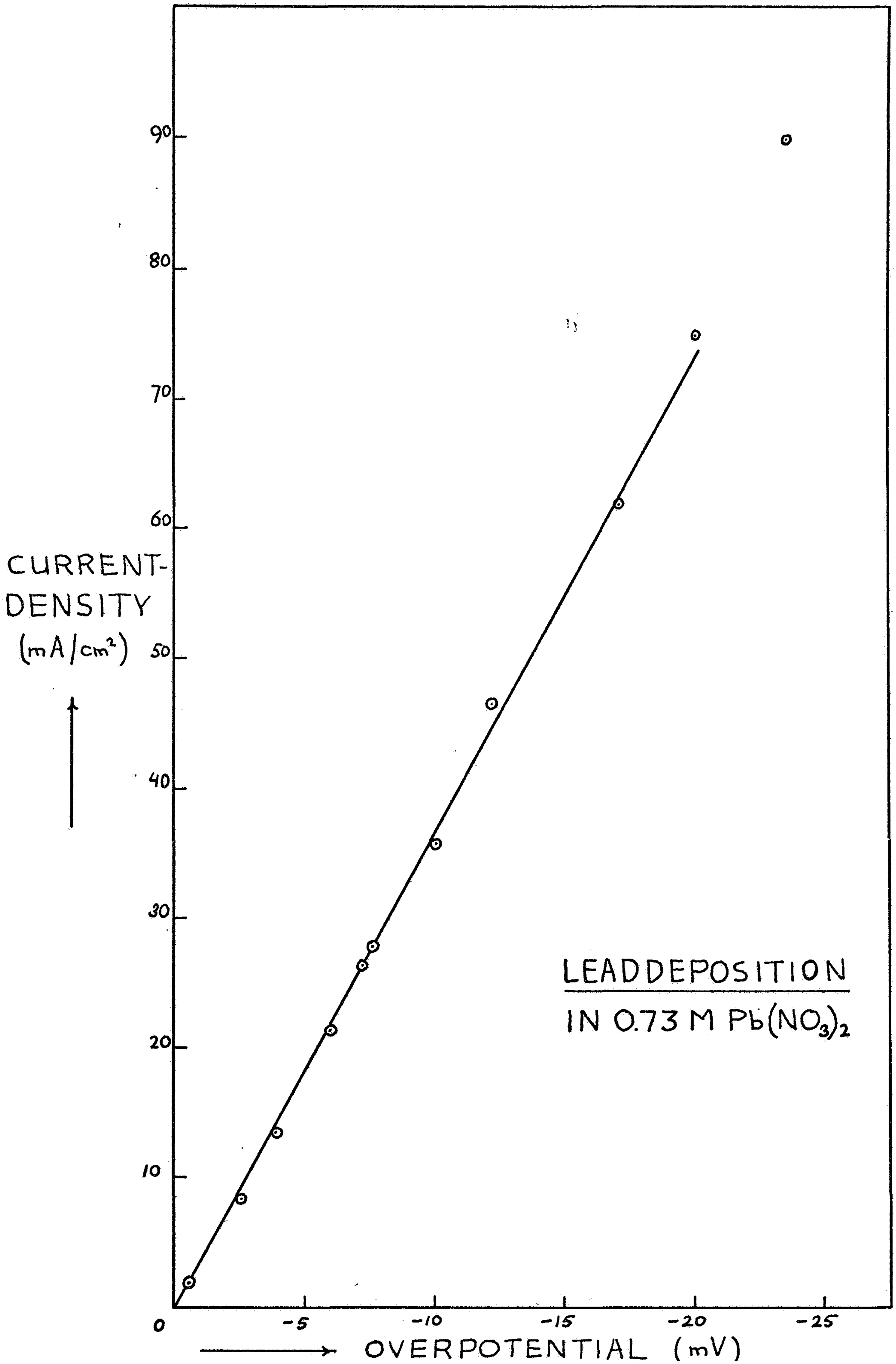
90
80
70
60
50
40
30
20
10
0
-5
-10
-15
-20
-25
CURRENT-DENSITY (mA/cm²)
OVERPOTENTIAL (mV)
LEADDEPOSITION
IN 0.73 M Pb(NO3)2

1.1.3.2. Appendix: mass transfer calculations

Grashof number calculations are shown in table 1 for the lead nitrate system (0.73M), the Cu SO_4-H_2SO_4-H_2O system table 2 and for saturated ZnO in 30% KOH table 3. By combining equation 2 with equation 3 of section 1.1.2.4, the Grashof number (8,10) is given as

$$Gr = \frac{g \alpha \Delta c h^3}{\nu^2}$$

<u>Table 1</u> data for lead deposition from $Pb(NO_3)_2$ solution, vertical electrode (h = 1 cm) 25°C

c_{bulk} mol /ℓ	ρ_{av} g/cm³	$\Delta\rho$ g/cm³	Δc mol /cm³	α cm³/mol	g cm/sec²	η cps	ν cm²/s	Gr
0.73	1.2166	0.0247	0.089×10^{-3}	230	10	1.6 (est.)	1.35×10^{-2}	9500

<u>Table 2</u> copper deposition from $CuSO_4$-H_2SO_4-H_2O, vertical electrode, h = 1 cm, 25°C

c_{bulk} mol /ℓ	ρ_{av} g/cm³	$\Delta\rho$ g/cm³	Δc mol /cm³	α cm³/mol	g cm/sec²	η cps	ν cm²/s	Gr
0.70	1.1861	0.1890	0.7×10^{-3}	238	10	1.76	1.49×10^{-2}	7190

<u>Table 3</u> zinc deposition from ZnO-KOH solution (battery charging), 25°C, vertical electrode (h = 1 cm)

c_{KOH} mol /ℓ	ρ_{KOH} g/cm³	c_{ZnO} mol /ℓ	ρ_{bulk} g/cm³	ρ_{av} g/cm³	$\Delta\rho$ g/cm³	Δc mol /cm³	α cm³/mol	g cm/sec²	η cps	ν cm²/sec	Gr
6.924	1.2936	0.690	1.3360	1.3148	0.0424	0.69×10^{-3}	47	10	2.53	1.91×10^{-2}	1235

1.1.3.3. References

(1) L. Gaines: Secondary silver-zinc battery technology. J. Electrochem. Soc. 116, 61C (1969).

(2) School of Chemical Engineering, University of Pennsylvania. Study of the zinc-silver oxide battery system. Contract No. 952-543 for JPL (quart. report July/Sept. 1970).

(3) P. Bro and H. Y. Kang: Discharge profiles in a porous cadmium electrode. Electrochem. Soc. Extended Abstract 67, Fall 1970 Meeting Atlantic City.

(4) Z. Stachurski: Investigation and improvement of zinc electrodes for electrochemical cells. Final report (1965) Contract No. NAS 5-3873, Yardney Electric Corp.

(5) J. E. Oxley: The improvement of zinc electrodes for electrochemical cells. Final report (1964), Contract No. NAS 5-3908, Leesona Moos Lab.

(6) S. Arouete and K. F. Blurton: The improvement of zinc electrodes for electrochemical cells. Final report (1966), Contract No. NAS 5-9591, Leesona Moss Lab.

(7) G. Wranglén: A shadow Schlieren method for the study of diffusion boundary layers at electrodes. Acta Chem. Scand. 12, 1543 (1958).

(8) C. R. Wilke, C. W. Tobias and M. Eisenberg: Free-convection mass transfer at vertical plates. Chem. Eng. Prog. 49,663 (1953).

(9) U. Böhm: Note on mass transfer by free convection at inclined electrodes by M. G. Fouad and A. M. Ahmed. Electrochim. Acta 15, 1841 (1970).

(10) C. R. Wilke, M. Eisenberg and C. W. Tobias: Correlation of limiting currents under free convection conditions. J. Electrochem. Soc. 100, 513 (1953).

(11) Handbook of Chemistry and Physics, 43 ed. The Chemical Rubber Co. (1966).

(12) M. Eisenberg, C. W. Tobias and C. R. Wilke: Selected physical properties of ternary electrolytes employed in ionic mass transfer studies. J. Electrochem. Soc. 103, 413 (1956).

(13) M. Eisenberg, H. F. Bauman and D. M. Brettner: Gravity field effects of zinc anode discharge in alkaline media. J. Electrochem. Soc. 108, 909 (1961).

(14) S. U. Falk and A. J. Salkind: Alkaline storage batteries. Wiley, New York (1969).

(15) U. Böhm, N. Ibl and A. M. Frei: Zur Kenntnis der natürlichen Konvektion bei der Elektrolyse in engen Räumen. Electrochim. Acta 11, 421 (1966).

(16) R. Piontelli, G. Poli and G. Serravalle: A contribution to the study of the electrode behavior of metallic single crystals. Transactions of the Symposium on Electrode Processes (1959) E. Yeager (ed.), p. 67 (1961).

2.1 Membrane Permeation

2.1.1 Steady State Experiments

2.1.1.1 A) Apparatus and Procedure

The rotating membrane apparatus described in previous reports has been improved and used for steady state determination of the permeability of ZnO through an acrylic-acid grafted and divinylbenzene cross-linked polyethylene membrane in 40% KOH solution. Problems initially encountered due to adapting the apparatus for operation in the corrosive and viscous alkali solutions have been solved. Neoprene "C" rings greased with Dow Corning FS 1281 lubricant were satisfactory in sealing the apparatus and providing smooth operation at rotational speeds up to 25 RPM. Dow Corning 111 lubricant was used as sealer and lubricant for the plastic components. Both lubricants have good chemical resistance and temperature stability (-40 to 500°F).

Steady state runs have been initiated with the membranes presoaked in either 40% KOH alone or in 0.4M ZnO in 40% KOH for 24 hours prior to the run, providing alternate initial concentration distribution of Zn in the membrane. After assembly of the apparatus, the chambers are filled with 40% KOH-0.4M ZnO and with 40% KOH respectively. A few drops of methylene blue are added to the zincate solution to allow easy visual determination of leaks. The disk speed is set at 13.1 RPM and the desired temperature maintained to 0.1°C by circulating water from a constant temperature bath through the jackets of the chambers. 1 ml samples are taken every 30 seconds for the first 2.5 minutes, and afterwards at 5 minute intervals. 1 ml of 40% KOH is replaced for each sample removed to maintain the chamber volume. Each run is continued for about one and a half hours.

B) Zinc Analysis

Improvements have been made to the analysis of zinc using the AA-120 atomic absorption spectrophotometer. Due to the viscosity of the KOH solutions, poor reproducibility and frequent clogging of the nebulizer in the AA-120 was observed. An extraction technique for zinc using Dithizone in carbon tetrachloride was found unsatisfactory for obtaining the reproducibility necessary. A method based on neutralization of the KOH and dilution to the optimal operating range of the AA-120 proved satisfactory. 1 ml of sample is added to 19 ml of 2.4% nitric acid and well mixed, neutralizing the alkali and reducing the viscosity of the resulting solution so that trouble free operation in the AA-120 is obtained. The 20 fold dilution of the Zn is still well within the sensitivity of the analysis. To reduce analytical error further, at least three aliquots of the diluted sample were sprayed into the machine consecutively, with the output recorded by a Leeds and Northrup Speedomax H recorder. The average value of the three readings was then used to determine Zn concentration by comparison with a standard calibration curve. A new calibration is prepared for each series of determination to eliminate errors due to changes in lamp and flame conditions.

2.1.1.2 Method for Analysis of Results

If two well mixed chambers with different concentrations of a permeant species are separated by a membrane, the concentration of permeant in the second chamber will increase with time. After an initial unsteady state period in which concentration gradients are established, a steady-state, or rather, pseudo steady-state period will ensue, which lasts as long as the concentration in the first chamber is much greater than that in the second. If we let

c_1 = concentration of permeant in chamber with volume V_1;

c_2 = concentration of permeant in chamber with volume V_2;

c_{10}, c_{20} = concentrations of permeant in chambers $_1$ and $_2$ at time zero;

K = overall mass transfer coefficient, including resistance of membrane and boundary layers on either side;

A = area of membrane available for permeation;

t = time;

then the overall mass balance is given by

$$c_1V_1 + c_2V_2 = c_{10}V_1 + C_{20}V_2$$

and the rate of change of permeant in the second chamber is given by

$$V_2\, dc_2/dt = KA(c_1 - c_2)$$

The solution to these equations is

$$\ell n \left[1 + \frac{(C_{20} - C_2)\ (1 + V_2/V_1)}{C_{10} - C_{20}}\right] = -KA\ (1/V_1 + 1/V_2)\ t$$

This result suggests that if the expression in brackets on the left is plotted versus time on semilogarithmic graph paper, a straight line will be obtained, whose slope is proportional to K, the desired overall coefficient. The overall coefficient is related to the membrane permeability by the relation

$$1/K = 1/K_m + 2/K_b$$

where K_m is the membrane permeability and K_b is the mass transfer coefficient in the boundary layer on either side of the membrane. Because of the special properties of the rotating disk membrane, K_b can be easily calculated from the known speed and properties of the solutions, allowing the calculation of K_m.

The method of sample taking, in which 1 ml of zinc free solution is replaced in the second chamber for each ml of sample taken results in the measured concentration of zinc in each sample being less than what would be obtained if no additions were made to maintain constant volume. Let

c_{2n} = concentration of zinc in second compartment at time n, if no sample had been taken

c'_{2n} = measured concentration of zinc in sample taken at time n, under actual conditions of replacing sample with equal volume of Zn free solution;

Then,

$$c_{2n} = c'_{2n} + (1/V_2) \sum_{m=1}^{n-1} c'_{2m}$$

2.1.1.3 Results and Discussion

Figure 1 shows the results of a typical steady state run, plotted as suggested by the analysis in the previous section. For this run, initial Zn concentration in the membrane was zero, with the concentration of Zn in the first chamber 0.4 M, and a temperature of 26.5° C. The concentration of Zn in the second chamber rose to 52μg/ml after one hour. Membrane area was 5.1 cm^2, with chamber volumes of 259 and 295 ml respectively. The dry membrane is 0.0012 inch thick.

We note that a leak developed in the membrane after about one hour, and that the technique was quite sensitive in detecting it. However, since steady state is obtained long before, a good value for overall permeability can be obtained. From the slope, a value of 3.50 x 10^{-5} cm/sec is calculated. The only previous value for the same membrane, obtained under similar conditions was 3.8 x 10^{-5}, as reported in the Feb. 1970 report. The newer value is considered much more reliable due to the improvements in operating technique and analysis recently instituted.

Experiments can now be reliably performed, and a program to measure permeabilities for a given membrane under varying conditions of concentration and temperature has been instituted. Measurement of the permeability temperature coefficient and comparison with diffusivity values in free solution, (reported on in section 2.2 of this report), will give insight into the mechanism of permeation and possible interaction of permeant and membrane, leading to development of membranes with improved permeation characteristics. Because, even with our improved technique, many time consuming determinations are needed for each membrane using the steady state technique,unsteady state methods in which the bulk concentrations are deliberately varied with time are being developed. This is discussed below in Sec. 2.1.2.

2.1.2 Unsteady State Experiments

2.1.2.1 Procedure

To decrease the number of separate runs needed to evaluate a given membrane, an impulse response technique for varying the solution concentrations is being developed. The procedure differs from the steady state runs in that initially both chambers are filled with 40% KOH with no zinc. To start the run, a given volume of solution is withdrawn from one compartment, and replaced by the same volume of solution containing zinc. The initial time is then accurately known. In the first trials, 10 ml of 0.4 M ZnO was introduced, and samples withdrawn from one compartment, and replaced by the same volume of solution containing zinc. The initial time is then accurately known. In the first trials, 10 ml of 0.4 M ZnO was introduced, and samples withdrawn from the second compartment every minute. Because of the low concentration in the first compartment compared to that used in the steady state runs, reproducibility was poor. In later runs, 50 ml of ZnO solution was used. The membrane speed was increased to 21.5 RPM to decrease the boundary layer resistance. A three-way stopcock is used for connecting 50 ml syringes to the inlet and exit ports, so that the solutions can be added and withdrawn rapidly. Mechanical stirring was used in each compartment to speed up mixing and insure that representative samples were obtained. Temperature was maintained at 21.5° C.

In theory, the permeability can be obtained from the unsteady state concentration change of Zn with time in the second compartment, for a given concentration in the first compartment which changes only very slowly with time. After sufficient samples have been taken to adequately describe the output curve, a second impulse of concentrated Zn colution can be added to the first compartment, and the permeability determined for the higher Zn concentration. In this way, permeabilities for the entire desired range of Zn concentrations can be obtained from a single run. Similarly, changes in temperature can be made during the run, so that the entire concentration-temperature variation of permeability for a single membrane can be obtained from a single run.

The concentration of ZnO in the first compartment is obtained as follows. Let

c'_{10} = concentration of Zn in first compartment before addition of V_r ml of ZnO solution containing M moles of Zn/liter

c_{10} = concentration of Zn in first compartment after the addition;

then

$$c_{10} = (1 - V_r/V_i)\, c'_{10} + (V_r/V_1)\, M$$

Thus, step changes of any size in Zn concentration can be obtained, limited only by the concentration M obtainable. To increase the size of the step, hot solutions, containing ZnO concentrations much greater than saturated at the temperature of the run, will be added in future runs.

2.1.2.2 Preliminary Results

Figure 2 gives the concentration of Zn in the second compartment during a preliminary run using the step response technique. Each discontinuity in slope corresponds to a step increase in ZnO concentration in the first compartment. During this single one and one-half hourrun, data for five different concentrations were obtained. It will be noted that scatter is high, making analysis difficult. This is due to imperfections in the technique, such as: too small changes in the size of the step; too small values in the volume of each step; and use of the same needles for adding and withdrawing samples which led to contamination between samples. These problems are eliminated by obtaining adequately size needles and syringes in sufficient quantity to enable completion of an entire run without having to reuse the same needles, and by adding hot solutions of higher Zn concentration. It is expected that complete results for the polyethylene membrane will be available for the next report.

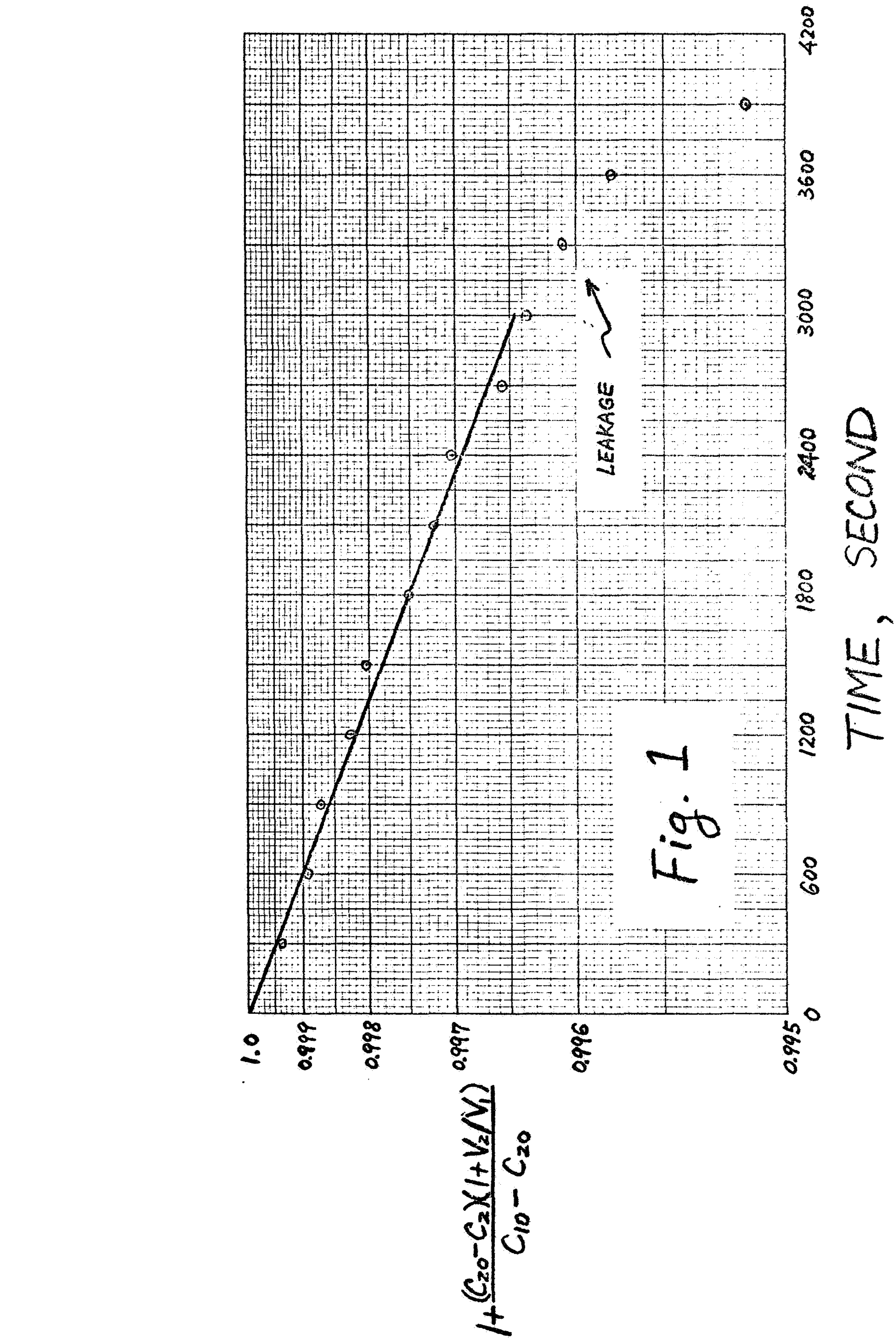
0
600
1200
1800
2400
3000
3600
4200
TIME, SECOND
1.0
0.999
0.998
0.997
0.996
0.995
$1+\frac{(C_{20}-C_2)(1+V_2/V_1)}{C_{10}-C_{20}}$
LEAKAGE

Fig. 1

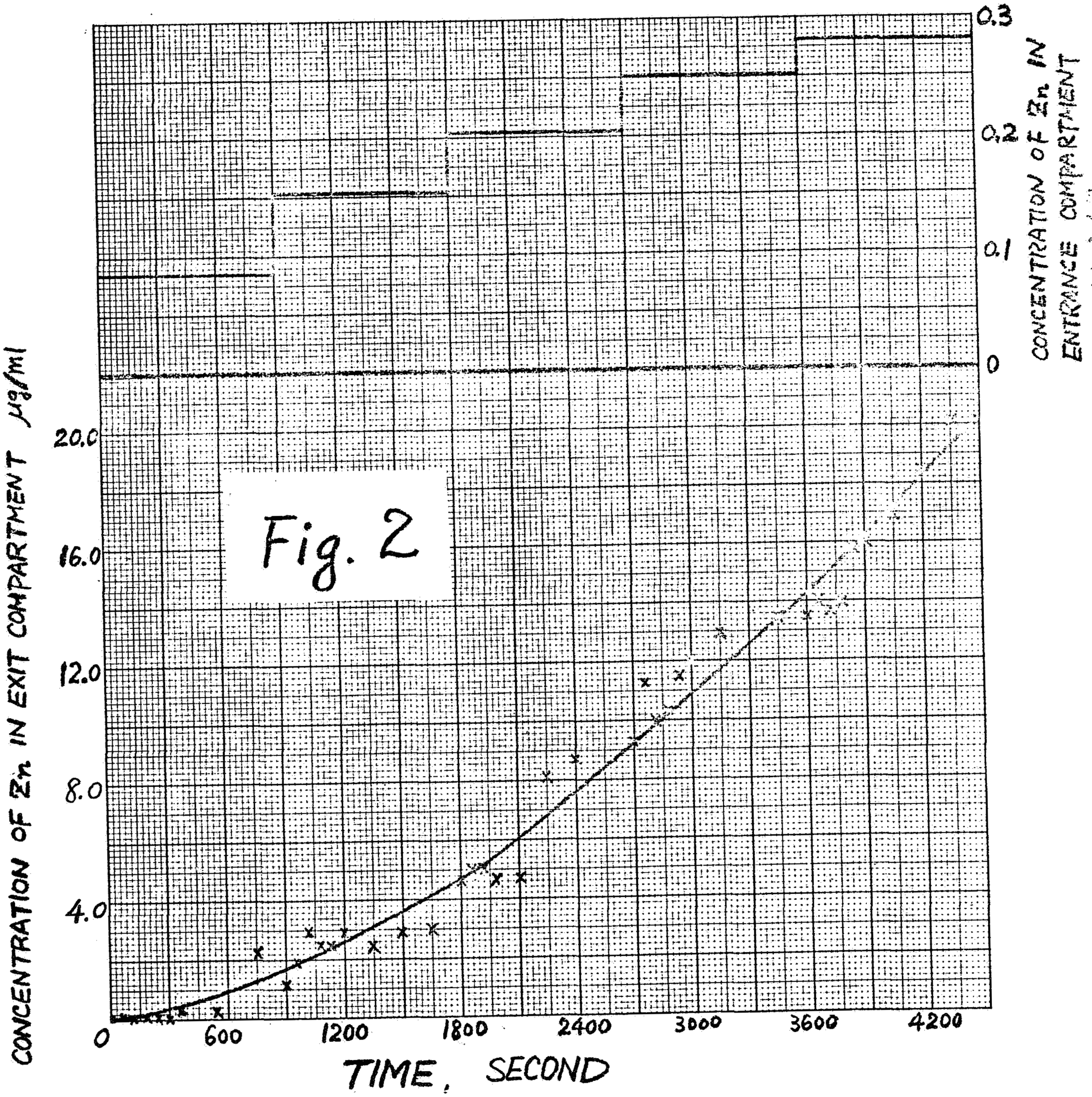
0.3
0.2
0.1
0
CONCENTRATION OF Zn IN
ENTRANCE COMPARTMENT
20.0
16.0
12.0
8.0
4.0
0
600
1200
1800
2400
3000
3600
4200
CONCENTRATION OF Zn IN EXIT COMPARTMENT μg/ml
TIME, SECOND

Fig. 2

2.2 Diffusivity of ZnO in 40% KOH Solution

2.2.1 Double Channel Apparatus

The double channel capillary apparatus described in the last report has been equipped with constant flow and temperature control, as shown in Figure 3. The main head tank provides constant flow to the apparatus, and is capable of flow rates as low as 10^{-2} ml/sec. The small constant level tank is used to maintain the level of solution above the capillaries. The temperature bath allows temperature in the apparatus to be controlled to within 0.1° C over a range from 15 to 40° C.

Since the volume of the capillaries must be accurately known to calculate diffusivity from this technique, volumes for all three sizes were determined. Each capillary was filled with mercury, and the meniscus flattened using the same screw apparatus used during a run(see report of Sec. 2.2 July-Sept.,1970. The capillaries were then weighed and compared with the empty weight. Typical values are as follows:

Small capillary: 0.0628 $\pm$ .0003 ml
Medium capillary: 0.0872 $\pm$ .0007 ml
Large capillary: 0.1096 $\pm$ .0007 ml

2.2.2 Flow Characteristics

In order to estimate the magnitude of the $\Delta \ell$ effect (see below) the linear velocity past the mouth of the capillary must be known. The following analysis was used to estimate this velocity for the capillary apparatus:

Assume that a parabolic velocity profile exists in the channel apparatus in both the vertical and horizontal directions, as shown. This is a reasonable assumption at the low velocities used. Let

v_c = centerline velocity in top view;

v_t = surface velocity in top view.

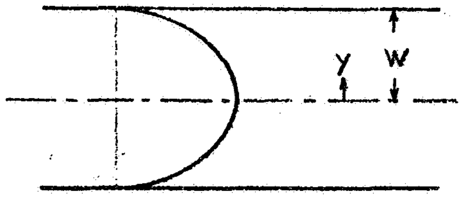

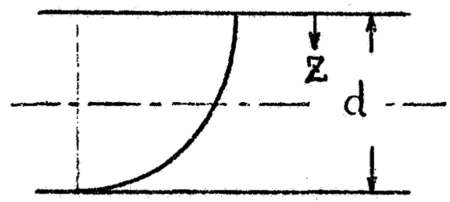

Then, for parabolic distributions,

$$v = v_t \left[1 - (z/d)^2\right] \left[1 - (y/w)^2\right]$$

and the average velocity in the channel is given by

$$v_{ave} = \frac{1}{A} \iint V dy dz$$

when the integrations are carried out. In terms of the volumetric flow rate Q, we have

$$v_t = (9/4)\ Q/A$$

where A is the cross section area of the channel.

For the apparatus used here, w = 2.3 cm; d = 2.6 cm; and the tops of the capillaries are located at position y = 0.7 cm and z = 1.3 cm. The linear velocity past the mouth of the capillary is then

$$V = 0.13Q$$

2.2.3 Reduction of $\Delta \ell$ Effect

According to the literature[1], the magnitude of the $\Delta \ell$ effect depends on the Reynolds number of the flow past the tip of the capillary. For Reynolds numbers less than unity the effect should be negligible. The lowest volumetric flow rate easily attainable in the present apparatus is about 10^{-2} ml/sec. Using the relationship for linear velocity obtained in the previous section, for this flow rate the linear velocity past the mouth of the capillary is 1.3×10^{-3} cm/sec. Because of the low velocity, small size and high viscosity, the Reynolds number is then much smaller than unity, so that the $\Delta \ell$ effect should be negligible.

It remains to be determined if the velocity is sufficient to achieve matching of the boundary condition used in solving the capillary diffusion equation, which is that the concentration at the mouth should be maintained the same as that of the bulk solution by adequate flow. A criterion for minimum required flow if given by

$$d^2 = 2D\Delta t$$

where d is the capillary diameter, D is the diffusivity of the solute, and Δt is the time available for diffusion. Therefore, the velocity past the mouth of the capillary should be

$$v = d/\Delta t \geq 2D/d$$

The apparatus will be checked using 1N KCl solution at 25° C, for which the diffusivity is 1.9×10^{-5} cm^2/sec. Capillary diameter is 0.2cm. Therefore, the velocity must be greater than 1.2×10^{-4} cm/sec. Since the actual velocity to be used is an order of magnitude greater, this condition will be achieved easily. Furthermore, since the diffusivity of zincate, based on our earlier results, is at least an order of magnitude less than the KCl, the condition will also be matched for the zincate determinations.

2.2.4 Optimization of Run Time

In using the capillary technique, sufficient time must elapse to allow reduction in average concentration of the diffusing species, so that accurate analysis can be made of the difference in concentration between the beginning and end of the experiment. However, to allow sufficient numbers of determinations, the runs should be kept as short as possible consonant with the first criterion. A good compromise would be to select a time such that the semi-infinite criterion would still be applicable. This is $Dt/L^2 < .06$, where D is diffusivity, t is time, and L is the capillary length. If this is met, then the time dependence of average concentration in the capillary is given by

$$1 - \frac{C_{ave}}{C_{init}} = \frac{2}{L}\sqrt{\frac{Dt}{\pi}}$$

For a 2.6 cm long capillary, the time for KCl diffusion by these formulas is about 6 hours. If run times of 5.5 hours are used, we would then have, for the short (2.6 cm) capillary

$$\frac{C_{ave}}{C_{init}} = 0.734$$

For the long (4.6 cm) capillary, we have

$$\frac{C_{ave}}{C_{init}} = 0.850$$

These changes are well within the accuracy of the analytic technique for zinc using the AA-120 spectrophotometer. Therefore, run times of about 5 hours will be standardized upon for the remainder of the diffusivity determinations.

2.2.5 References and Figures

(1) L. Nanis, S. R. Richards and J. O'M. Bockris, The $\Delta\ell$ Effect in Capillary-Reservoir Diffusion Measurements, Rev. Scient. Instr. 36, 673-677 (1965).

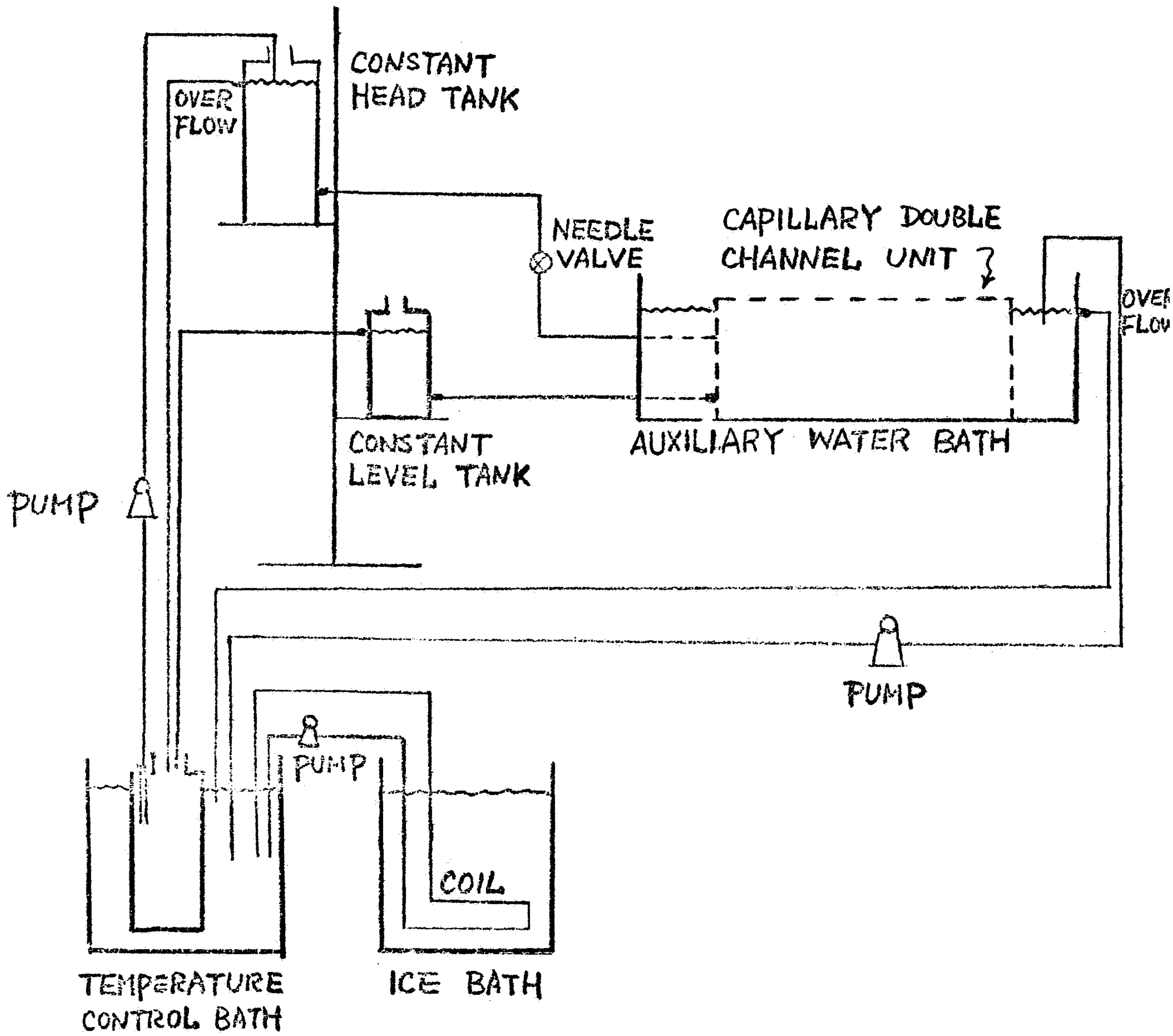
CONSTANT
HEAD TANK
OVER
FLOW
NEEDLE
VALVE
CAPILLARY DOUBLE
CHANNEL UNIT
OVER
FLOW
CONSTANT
LEVEL TANK
AUXILIARY WATER BATH
PUMP
PUMP
PUMP
COIL
TEMPERATURE
CONTROL BATH
ICE BATH

Fig. 3